Journal of Membrane Science 350 (2010) 259–268

Contents lists available at ScienceDirect

Journal of Membrane Science

journal homepage: www.elsevier.com/locate/memsci

A new theoretical gas permeability model using resistance modeling for mixed matrix membrane systems

S.A. Hashemifard [a,1], A.F. Ismail [a,*], T. Matsuura [b,2]

[a] Advanced Membrane Technology Research Centre (AMTEC), Universiti Teknologi Malaysia, 81310 UTM Skudai, Johor Darul Ta'zim, Malaysia
[b] Industrial Membrane Research Institute, Department of Chemical and Biological Engineering, University of Ottawa, 161 Louis Pasteur St., Ottawa, ON, K1N 6N5, Canada

ARTICLE INFO

Article history:
Received 2 November 2009
Accepted 26 December 2009
Available online 7 January 2010

Keywords:
Gas permeability
Mixed matrix membrane
Prediction
Resistance modeling

ABSTRACT

This paper discusses the development of a new theoretical model based on resistance modeling approach to predict mixed matrix membrane (MMM) performance. To develop the proposed model, the element of MMM is considered as a unit cell of body centered cubic (BCC). The network of permeation resistances are developed based on this unit cell. The main parameters considered and discussed are: dispersed filler loading, polymer matrix permeability, dispersed filler permeability, interphase permeability and interphase thickness. The results generated from the proposed model have been verified using seven cases through the published experimental data. Excellent *agreement* has been obtained in most cases between the model results and the selected published values. Thus, the newly proposed model is capable in predicting the permeability and selectivity for all known MMM morphologies.

1. Introduction

Polymers are the materials more widely used for membrane manufacturing in virtue of their high processability, good intrinsic transport properties and low cost. On other hand, inorganic materials present strong capability to discriminate gas species even in severe temperature and pressure conditions and aggressive environments. However, their use is still limited due to the problems in reproducibility in the preparation step, as well as short lifetime and high cost [1–3]. Mixed matrix membranes (MMMs) are heterogeneous membranes that consist of inorganic fillers dispersed in a polymer matrix [4–24]. The concept of MMM combines the advantages of each phase: high selectivity of the dispersed fillers and desirable mechanical properties and economical advantages of polymers. MMMs are very effective in gas separation processes (for example: separation of oxygen–nitrogen mixture, purification of natural gas by removing carbon dioxide). The inorganic fillers used in MMMs are mostly porous molecular-sieve type materials, including zeolites [13–15] and carbon molecular sieves [5,11,25]. The incorporation of molecular-sieve type fillers in polymer matrix generally leads to higher permeability, higher selectivity, or both compared to the polymeric membrane, since the molecular-sieve type fillers used in MMMs are capable of discriminating between different molecules present in the feed mixture, usually on the basis of size and shape of molecules. For example, in the separation of oxygen–nitrogen mixture zeolite NaA is very effective as a molecular-sieve filler [14]. Carbon molecular sieves (CMSs) are also important as inorganic filler materials for MMMs. Gas separation in CMS materials is based on the difference in adsorption kinetics of different molecular species; i.e. oxygen molecules adsorb more quickly on CMS than nitrogen molecules, thus permeate through the CMS membrane faster [5].

The proper theoretical description and modeling of the permeability of composite membranes such as MMMs are of great interest, particularly in view of the growing technological importance of these membranes. Mathematically, gas transport through a mixed matrix medium presents a complex problem. Attempts were made to predict the performance of MMMs by various theoretical expressions, including models by Maxwell (1873), Bruggeman [33], Lewis–Nielsen, Pal and Felske [26,27]. The principles of applying flow resistances in series and parallel in order to describe gas permeation through asymmetric membranes were first outlined by Henis and Tripodi [28], who predicted that a defective membrane for gas separation owing to the presence of surface pores or imperfections could exhibit gas separation properties close to the capabilities of the solid polymer once coated with silicone. They applied the resistance approach to typical membrane structures and made assumptions as to the nature of the deposition of the coating material (e.g. the thickness of the silicone rubber layer and pore penetration depth). The performance of these hypothetical coated membranes was thus predicted. Fouda et al. [29] pointed out the limitations in the Henis and Tripodi model when fitting actual gas

* Corresponding author. Tel.: +60 7 5535592; fax: +60 7 5581463.
E-mail address: afauzi@utm.my (A.F. Ismail).
[1] Tel.: +60 7 5535592; fax: +60 7 5581463.
[2] Tel.: +1 613 562 5800x6114; fax: +1 613 562 5172.

0376-7388/$ – see front matter © 2010 Elsevier B.V. All rights reserved.
doi:10.1016/j.memsci.2009.12.036

permeation results. They then introduced the Wheatstone bridge model which could better explain the permeation data. Karode et al. have proposed an improved Wheatstone bridge resistance model for diffusion through a thin film composite (TFC) membrane [30]. The constriction resistance encountered by the diffusing species in seeking out a pore in the support membrane to diffuse through was quantified. Funk and Lloyd introduced the concept of zeolite-filled microporous mixed matrix membranes, referred to as ZeoTIPS membranes, and discussed their potential use for gas separations [31]. ZeoTIPS membranes, which are formed using the thermally induced phase separation (TIPS) process, consist of zeolite particles supported in a microporous polymer matrix. In addition to discussing the preparation of ZeoTIPS membranes and their structures, their paper presented a model using resistance modeling approach that could be used to demonstrate the potential of these membranes in gas separation applications. The model depended on the zeolite loading and the ratio of void volume to polymer volume in the membrane.

In the current paper, some of the existing models for predicting the permeation properties of MMMs are first briefly reviewed. Then, a new theoretical model for MMM is developed based on resistance modeling approach. Moreover, the results generated from the proposed model were tested by comparing calculated results with experimental values reported in the literature. To the best of our knowledge, the comparison was scarcely discussed in the open literature.

2. Existing permeation models

Few of representative models are described below. The existing models for permeation through MMMs are adaptations of thermal/electrical conductivity models. Due to close analogy between thermal/electrical conduction and permeation of species through composite materials, the conductivity models are readily adaptable to permeability of species in MMMs. The existing models for permeation through MMMs are adaptations of thermal/electrical conductivity models. In most cases, attempts are made to predict the permeability of MMMs based on the permeabilities of the continuous phase (polymer matrix) and the dispersed phase (filler particles).

The Maxwell model [32], originally developed for electrical conductivity of particulate composites, can be adapted to permeability as:

$$P_r = \frac{1 + 2\phi(\lambda_d - 1)/(\lambda_d + 2)}{1 - \phi(\lambda_d - 1)/(\lambda_d + 2)} \tag{1}$$

where P_r is the permeability ratio P/P_m, P is the effective permeability of MMM, P_m is the permeability of the continuous phase, ϕ is the volume fraction of the dispersed phase, known as loading, and λ_d is the permeability ratio P_d/P_m where P_d is the permeability of the dispersed phase.

The Bruggeman model [33], originally developed for the dielectric constant of particulate composites using the differential effective medium approach, can be adapted to permeability as:

$$(P_r)^{1/3}\left(\frac{\lambda_d - 1}{\lambda_d - P_r}\right) = (1 - \phi)^{-1} \tag{2}$$

While the Bruggeman model is an improvement over the Maxwell model, as far as the effect of ϕ is concerned, it has limitations similar to that of the Maxwell model.

The Lewis–Nielsen model [34], originally proposed for the elastic modulus of particulate composites, can be adapted to permeability as:

$$P_r = \frac{1 + 2\phi(\lambda_d - 1)/(\lambda_d + 2)}{1 - \psi\phi(\lambda_d - 1)/(\lambda_d + 2)} \tag{3}$$

where

$$\psi = 1 + \left(\frac{1 - \phi_M}{\phi_M^2}\right)\phi \tag{4}$$

where ϕ_M is the maximum amount of ϕ, which usually is considered equal to 0.64.

The Pal model [35], originally developed for thermal conductivity of particulate composites using the differential effective medium approach taking into consideration the packing difficulty of filler particles, can be adapted to permeability as:

$$(P_r)^{1/3}\left(\frac{\lambda_d - 1}{\lambda_d - P_r}\right) = \left(1 - \frac{\phi}{\phi_M}\right)^{-\phi_M} \tag{5}$$

Note that when $\phi_M \to 1$, the Pal model reduces to the Bruggeman model.

A modified Felske model was introduced by Pal [26,27] as:

$$P_r = \frac{1 + 2\phi(\beta - \gamma)/(\beta + 2\gamma)}{1 - \psi\phi(\beta - \gamma)/(\beta + 2\gamma)} \tag{6}$$

where β and γ are given in Eqs. (7) and (8):

$$\beta = (2 + \delta^3)\lambda_d - 2(1 - \delta^3)\lambda_i \tag{7}$$

$$\gamma = 1 + 2\delta^3 - (1 - \delta^3)\lambda_{di} \tag{8}$$

where δ is the ratio of outer radius of interphase to particle radius, λ_i is the ratio of interphase permeability to continuous phase permeability, and λ_{di} is the ratio of dispersed filler permeability to interphase permeability. In addition, the modified Felske model reduces to the Maxwell model when $\delta = 1$, that is, when the interfacial layer is absent. The Felske model has the same limitations as that of the modified Maxwell model. It is valid only when the volume fraction of dispersed filler particles ϕ is small.

One can model the three-phase (continuous, dispersed and interphase) MMM as a pseudo two-phase MMM with the continuous being one phase and the combined dispersed and interphase being the other phase (called combined phase hereafter) [6]. Models for these more complicated systems are based on 'nested applications' of the Maxwell or Lewis–Nielsen models. The Maxwell or Lewis–Nielsen model is first applied to know the permeability of the combined phase from the individual permeability of dispersed- and interphase. The permeability of the whole MMM is then calculated by applying these models for the second time to the permeability of the continuous and the combined phase. In this application the following volume fraction is necessary:

$$\phi_S = \frac{\phi}{\phi + \phi^i} \tag{9}$$

where ϕ_S is the volume fraction of the dispersed phase in the combined phase, and ϕ^i is the volume fraction of the interphase in the whole MMM.

The predicted ideal selectivity of the mixed matrix membrane for a gas pair is simply the ratio of effective permeabilities of two competing gas penetrants. For a mixture consisting of penetrants 1 and 2 it is:

$$\alpha_{1/2} = \frac{P_1}{P_2} \tag{10}$$

Also, there are other models in the literature such as those of Bottcher [36], Higuchi and Higuchi [37], and Looyenga [7]. Recently Hashemifard et al. focused on the evaluation of several of the present models in detail [38].

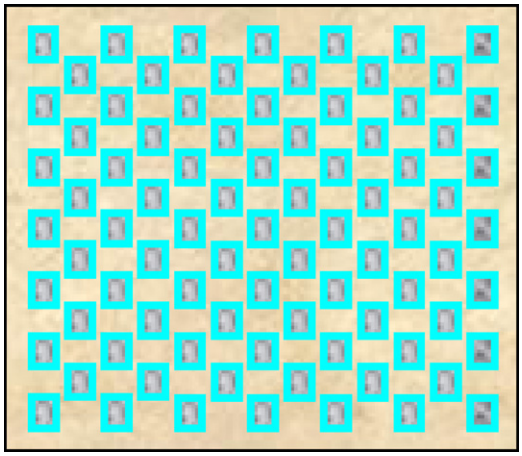

Fig. 1. BCC structure considered for particle distribution in MMM.

3. Theory of the proposed model

3.1. Mixed matrix membrane element description

In this work, permeability of MMM is theoretically modeled by the aid of a combination of simple series-parallel gas flow arrangement. It is known that the filler particles in MMMs are distributed randomly throughout the polymer matrix. Since researchers are attempting to distribute filler particles as uniformly as possible while preparing MMMs, a body centered cubic (BCC) lattice is selected to exhibit the particle distribution throughout a MMM, as illustrated in Fig. 1.

The smallest part that has the characteristics of the rest of the lattice is known as the unit cell. The unit cell of a BCC structure is a cube or a cuboid, containing eight particles in the corners and one particle in the centre (see Fig. 2). As it is clear, seven other cubes from the neighboring unit cells share the particle in every corner. Therefore, every BCC unit cell has a net total of two particles per unit cell ($8 \times 1/8 + 1$).

Here, the dispersed filler particle is considered to be a cylinder having height, d_l that is equal to diameter, d_r. If we further consider a sphere, with a diameter of d_p, whose volume is equal to that of the cylinder, the relationships between these three lengths are given by the following equations:

$$d_l = \sqrt[3]{\frac{2}{3}} d_p \tag{11}$$

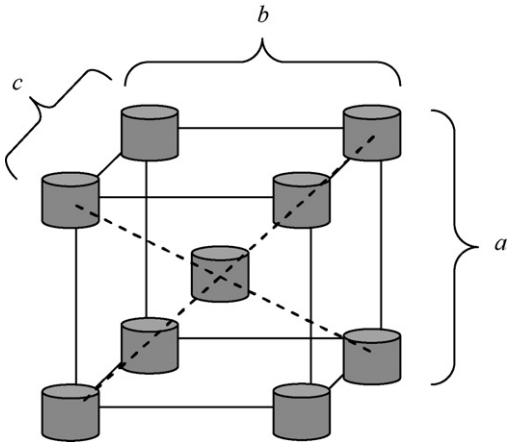

Fig. 2. Unit cell of BCC structure considered for particle distribution in MMM.

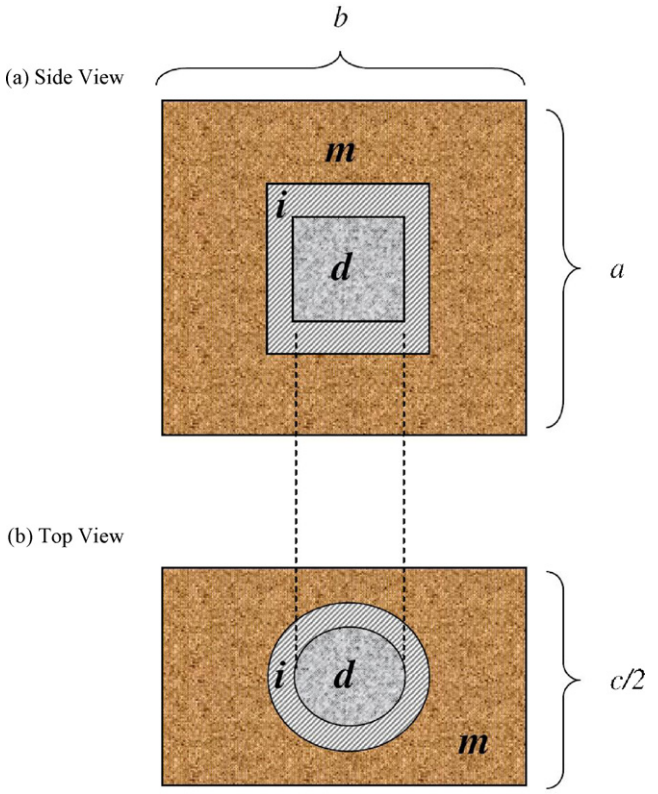

Fig. 3. Side (a) and top (b) view of the half BCC unit cell where a cylindrical particle is placed.

$$d_r = d_l \tag{12}$$

Petropoulos [39] showed that as far as the aspect ratio of the particles is close to unity, the effect of the particle shapes can be ignored easily. Moreover, the application of the parallel-series model becomes much easier for the cylindrical shape as will be shown later.

It should be noted that the unit cell is no longer a perfect cube but a cuboid having dimension of $a \times b \times c$, because of the specific shape of equal height and diameter of the cylindrical particle. However, we still call it a BCC unit cell, since "C" can stand for cuboid as well. The packing factor or maximum loading, ϕ_M, of the unit cell where the cylindrical particles start to touch each other is equal to 0.393. For this case, considering equal height and diameter of the cylindrical particle, the relation between the dimensions of the unit cell and the particle will be $a = 2d_l$ and $b = c = \sqrt{2}d_l$, hence, $b/a = c/a = \sqrt{2}/2$. This relationship is considered to hold even for the case when the volume fraction of the particles is less than ϕ_M.

Fig. 3 shows the side and top view of the half BCC unit cell where a cylindrical particle is placed. Since one whole BCC unit cell is occupied by two particles, only a half cell is enough to accommodate one particle. Hence the dimension of the half cell given in Fig. 3 is $a \times b \times (c/2)$ or $a \times (a/\sqrt{2}) \times (a/2\sqrt{2})$. The half cell containing a cylinder is hereafter called the MMM element.

It should be further noted that the MMM element shown in Fig. 3 consists of three separate phases; i.e. (i) the continuous phase (polymer matrix) (m), (ii) dispersed phase (filler particle) (d) and (iii) interphase (i). The continuous phase is a polymer matrix where the filler particles (dispersed phase) are embedded in. The interphase is a phase that results from the way in which polymer matrix and filler particle are attached to each other. Depending on the interaction between the polymer phase and the filler particle, various kinds of interphase morphologies may arise. Moore and Koros [40] have described four main possible morphologies with support of

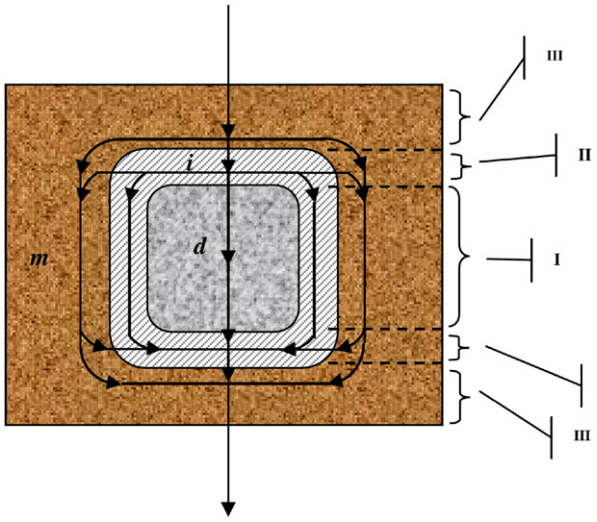

Fig. 4. Penetrant gas flow path through MMM element for void in MMM morphology.

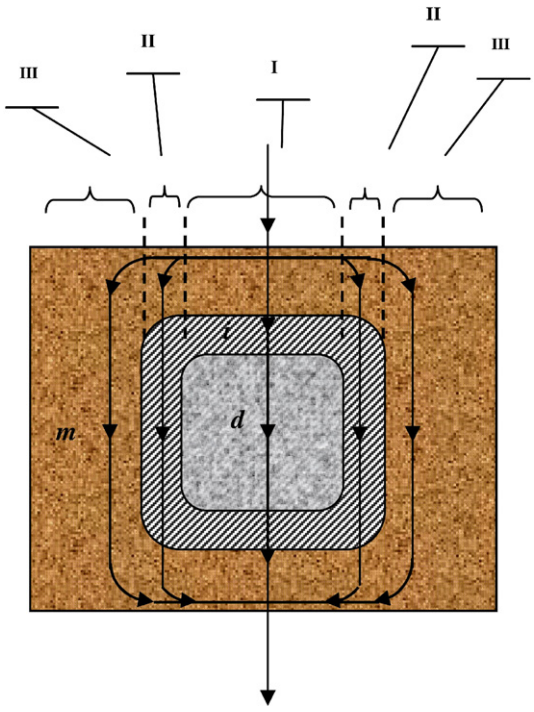

Fig. 5. Penetrant gas flow path through MMM element for rigidified MMM morphology.

experimental observations. Those morphologies are: (i) ideal contact between the matrix and the filler particle, known as ideal MMM. This morphology leads to an increase in both permeability and selectivity. However, it is hardly achievable. (ii) Rigidified polymer layer around the filler particle, known as rigidified MMM. This morphology leads to a decline in permeability of the penetrant gas by a factor of β, while selectivity experiences an increase. (iii) Sieve in cage morphology arises from the weak interaction between polymer matrix and filler, which is hereafter called void in MMM. This morphology, opposite to rigidified MMM, causes an increase in permeability and a dramatic decrease in selectivity. A special case of void in MMM is when the effective void thickness is an order of magnitude larger than the size of the diffusing gases, known as leaky MMM. (iv) Blocked sieve surface morphology, known as blockage in MMM. In this morphology, the pore entrance of the filler particle is blocked or semi-blocked by polymer functional groups or solvent molecules during dope preparation stage. Therefore the penetrant gas permeability through the dispersed particle is reduced by a factor of β'. More details about the interphase morphologies are discussed elsewhere [6,40].

3.2. Developing the new model using resistance modeling approach

The newly developed model is based on the flow patterns of the permeant gas through the MMM element shown in Fig. 4 (series of parallel flow) and Fig. 5 (parallel of series flow). It will be showed later, that the experimental data are in a good agreement with this pattern of gas flow through the MMM element. This reveals that, the proposed model is capable to give a useful tool to understand more about the gas flow behavior and hence distinguishing the differences between the morphologies and their influences on gas permeabilities in MMM. In Fig. 4, the gas permeates progressively through zone III, consisting of continuous phase only, then through zone II, consisting of continuous and interphase as a parallel channel, and finally through zone I, consisting of continuous, interphase and dispersed phase as a parallel channel. After zone I, the flow through zones II and III is repeated before the gas leaves the MMM element. In Fig. 5, the gas permeates through zone III, consisting of continuous phase only, and through zone II, consisting of continuous and interphase as a series channel, as well through zone III, consisting of continuous, interphase and dispersed phase as a series channel. The flow through each zone is parallel to each other. The flows through different zones are finally combined before leaving the MMM element.

The volume fractions defined below are required for the proposed model.

(a) volume fractions of zones I, II and III (ϕ_{I}, ϕ_{II} and ϕ_{III}) in the entire MMM element:

$$\phi_{\mathrm{I}} = \frac{\phi}{\pi\phi'^2} \tag{13}$$

$$\phi_{\mathrm{II}} = 2^{2/3}3^{1/3}\phi'\theta \tag{14}$$

$$\phi_{\mathrm{III}} = 1 - \phi_{\mathrm{I}} - \phi_{\mathrm{II}} \tag{15}$$

(b) volume fractions of dispersed phase, interphase and continuous phase in zone I:

$$\phi_{d\mathrm{I}} = \pi\phi'^2 \tag{16}$$

$$\phi_{i\mathrm{I}} = 4\sqrt[3]{\left(\frac{3}{2}\right)^2}\pi\phi'^2\left(\theta^2 + \sqrt[3]{\frac{2}{3}}\theta\right) \tag{17}$$

$$\phi_{m\mathrm{I}} = 1 - \phi_{d\mathrm{I}} - \phi_{i\mathrm{I}} \tag{18}$$

(c) volume fraction of interphase and continuous phase in zone II:

$$\phi_{i\mathrm{II}} = \sqrt[3]{\left(\frac{3}{2}\right)^2}\pi\phi'^2\left[\sqrt[3]{\left(\frac{2}{3}\right)^2} + 4\theta^2 + 4\sqrt[3]{\frac{2}{3}}\theta\right] \tag{19}$$

$$\phi_{m\mathrm{II}} = 1 - \phi_{i\mathrm{II}} \tag{20}$$

where

$$\phi' = \sqrt[3]{\frac{\phi}{\pi}} \tag{21}$$

$$\theta = \frac{t}{d_p} \tag{22}$$

ϕ is the volume fraction of dispersed phase in the total MMM element, t is the thickness of the interphase and d_p is given in Eq. (11).

It should be noted that the above volume fractions are not totally independent from each other. For example, by combining Eqs. (16), (17) and (19), ϕ_{iII} becomes:

$$\phi_{iII} = 4\phi_{dI} + \phi_{iI} \tag{23}$$

Noting that the overall permeance P can be obtained from the permeance P_j of an individual phase j with a volume fraction of ϕ_j; for a series combination, of the phases:

$$\frac{1}{P} = \sum_{j=1}^{n} \frac{\phi_j}{P_j} \tag{24}$$

and for a parallel combination of the phases:

$$P = \sum_{j=1}^{n} \phi_j P_j \tag{25}$$

Regarding the applicability of the above two models, the first model (parallel-series) seems applicable when the interphase is leaky, since the penetrant gas readily goes into the interphase after going through zone I of continuous phase, while the second model (series-parallel) seems applicable when the interphase is rigidified since the penetrant gas tends to avoid the zones II and III that include hard rigidified interphase. This creates a separate flow through a channel that consists of continuous phase only (zone I in Fig. 5).

And using the volume fractions defined above, the overall permeance P of the MMM element can be written uniformly as:

$$P = \left(\frac{\phi_{III}}{P_m^u} + \frac{\phi_{II}}{\phi_{iII} P_i^u + \phi_{mII} P_m^u} + \frac{\phi_I}{\phi_{dI} P_d^u + \phi_{iI} P_i^u + \phi_{mI} P_m^u} \right)^{-u} \tag{26}$$

where $u = 1$ is for the parallel-series combination (void and leaky interphase) and $u = -1$ is for series-parallel combination (rigidified interphase).

Dividing both sides of Eq. (26) by P_m yields:

$$P_r = \left(\phi_{III} + \frac{\phi_{II}}{\phi_{iII} \lambda_i^u + \phi_{mII}} + \frac{\phi_I}{\phi_{dI} \lambda_d^u + \phi_{iI} \lambda_i^u + \phi_{mI}} \right)^{-u} \tag{27}$$

where

$$P_r = \frac{P}{P_m} \tag{28}$$

Further substituting equivalents of ϕ_{III} (Eq. (15)), ϕ_{mII} (Eq. (20)) and ϕ_{mI} (Eq. (18)) in Eq. (27), we can obtain the final form of the proposed model:

$$P_r = \left[1 + \phi_{II} \left(\frac{1}{\phi_{iII} \left(\lambda_i^u - 1 \right) + 1} - 1 \right) + \phi_I \left(\frac{1}{\phi_{dI} \left(\lambda_d^u - 1 \right) + \phi_{iI} \left(\lambda_i^u - 1 \right) + 1} - 1 \right) \right]^{-u} \tag{29}$$

where λ_i and λ_d are, respectively, P_i/P_m and P_d/P_m, which are the ratios of interphase permeance and dispersed phase permeance to the permeance of the continuous phase. It should be noted that the above model was derived from the MMM structure and morphologies, while the models discussed in Section 2 were derived from thermal or electrical analogues. Accordingly, it may be possible to apply the newly developed model to predict other desired properties for composite materials.

Eq. (29) can be easily simplified for some special cases.

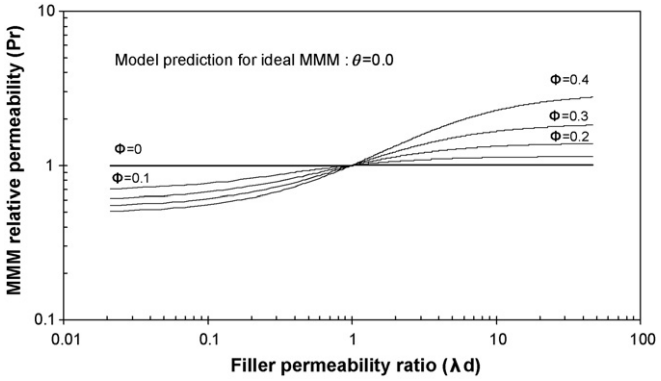

Fig. 6. Effect of dispersed filler permeability ratio and filler loading on relative permeability for ideal MMM.

For ideal morphology, there is no interphase. Then, $\phi_{II} = \phi_{iI} = \phi_{iII} = 0$, hence:

$$P_r = \left[1 + \phi_I \left(\frac{1}{\phi_{dI} \left(\lambda_d^u - 1 \right) + 1} - 1 \right) \right]^{-u} \tag{30}$$

Furthermore, for a series combination of continuous and dispersed phase, where the dispersed phase is sandwiched between two continuous phases horizontally, $\phi = \phi_I$, $\phi_{dI} = 1$ and $u = -1$ hence:

$$P_r = \frac{\lambda_d}{\phi + \lambda_d (1 - \phi)} \tag{31}$$

and for a parallel combination of continuous and dispersed phase, where the dispersed phase is sandwiched between two continuous phases vertically, $\phi = \phi_I$, $\phi_{dI} = 1$ and $u = 1$ hence:

$$P_r = \phi \lambda_d + (1 - \phi) \tag{32}$$

4. Results and discussions

4.1. Prediction of the proposed model

Since there are only four independent variables, i.e. ϕ, θ, λ_d,λ_i, involved in Eqs. (13)–(32), P_r can be written as a function of those variables, as:

$$P_r = f(\phi, \theta, \lambda_d, \lambda_i) \tag{33}$$

Some model calculations were made for various combinations of the variables. Note that parallel-series model was used when the interphase is void or leaky and series-parallel model is used when the interphase is rigidified.

(a) *For ideal MMM*: For this special case, $\theta = 0.0$. Furthermore, there is no λ_i. Hence, it is the function of ϕ and λ_d. Fig. 6 shows such a functional relationship. For a given ϕ, P_r changes only in a range $5 \times 10^{-1} < \lambda_d < 5 \times 10^{1}$, and hardly shows any change outside of the range. P_r is lower than unity when $\lambda_d < 1$ and higher than unity when $\lambda_d > 1$. P_r decreases with an increase in ϕ for $\lambda_d < 1$ and increases with an increase in ϕ for $\lambda_d > 1$. Therefore, only fillers with $\lambda_d > 1$ are acceptable to be applied for MMM.

(b) *For rigidified MMM*: The thickness of the interphase, t, is no longer zero. The permeability of interphase is less than that of the continuous phase since the polymer in the interphase is rigidified. These are represented by fixed dimensionless parameters $\theta = 0.1$ and $\lambda_i = 0.333$. P_r is shown as a function of ϕ and λ_d in Fig. 7. P_r decreases as ϕ increases. The effect is more pronounced for $\lambda_d < 1$.

(c) For leaky MMM and void in MMM, two sets of fixed parameters; i.e. $\theta = 0.0006$, $\lambda_i = 1000$ and $\theta = 0.2$, $\lambda_i = 10{,}000$ are used. λ_i values

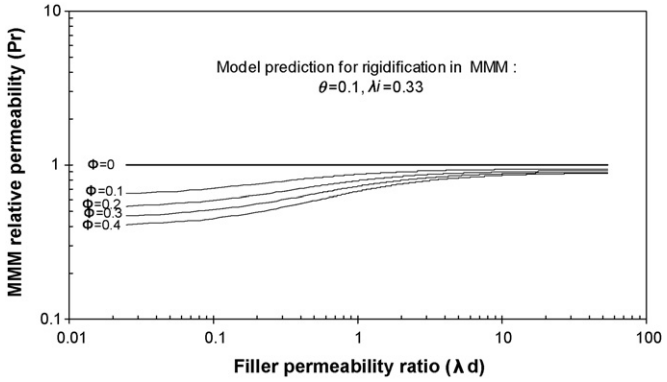

Fig. 7. Effect of dispersed filler permeability ratio and filler loading on relative permeability for rigidified MMM.

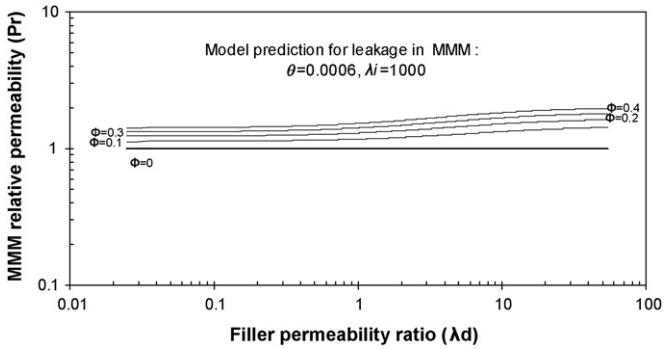

Fig. 8. Effect of dispersed filler permeability ratio and filler loading on relative permeability for leaky MMM.

are much larger than unity since the gas leaks the interphase which is the empty void. The second case represents a much larger void than the first case. P_r is shown as a function of ϕ and λ_d in Figs. 8 and 9.

P_r increases with an increase in ϕ. The effect is more pronounced for the second case (Fig. 9) and λ_d has hardly any effect on P_r, particularly in Fig. 9. Therefore, if an increase in permeability is the only desired effect, e.g. in the case of membranes for membrane contactor, any fillers can be used regardless of their intrinsic permeabilities.

(d) For rigidified MMM and void in MMM, two sets of fixed parameters are used; i.e. $\phi = 0.3$, $\lambda_i = 0.33$ and $\phi = 0.3$, $\lambda_i = 10$. Obviously, the first case represents rigidified MMM and the second void in MMM. P_r is shown as a function of θ and λ_d in Fig. 10. Depending on λ_i, θ has two different effects. P_r may either decrease ($\lambda_i = 0.33$) or increase ($\lambda_i = 10$) as θ increase. From Fig. 10, one may also observe that the effect of λ_d becomes less significant at higher θ values.

(e) For comparison of rigidified, ideal and void in MMM, ϕ and θ are set equal to 0.3 and 0.1, respectively. λ_i is changed from 0.4 (rigidified MMM) to 1.0 (ideal MMM) and further to 5.0 (MMM) and 1000 (void in MMM). Even though $\theta = 0.1$, ideal MMM can still be represented by setting $\lambda_i = 1.0$. P_r is shown as a function of λ_d in Fig. 11. From the figure, the order in P_r is rigidified MMM < ideal MMM < void in MMM.

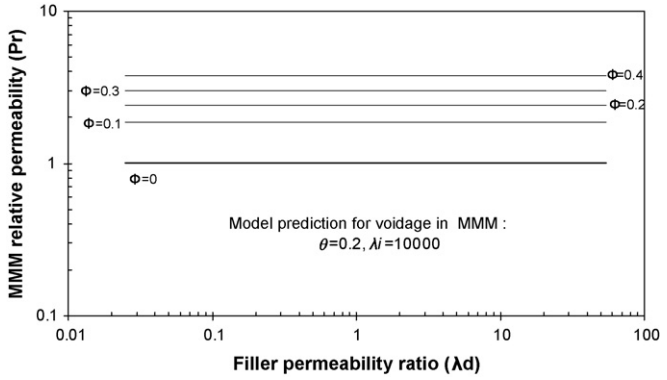

Fig. 9. Effect of dispersed filler permeability ratio and filler loading on relative permeability for void in MMM.

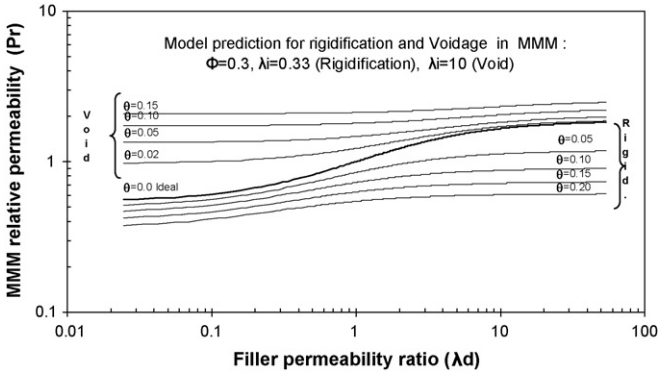

Fig. 10. Effect of dispersed filler permeability ratio and interphase thickness to particle diameter ratio on relative permeability for rigidified and void in MMM.

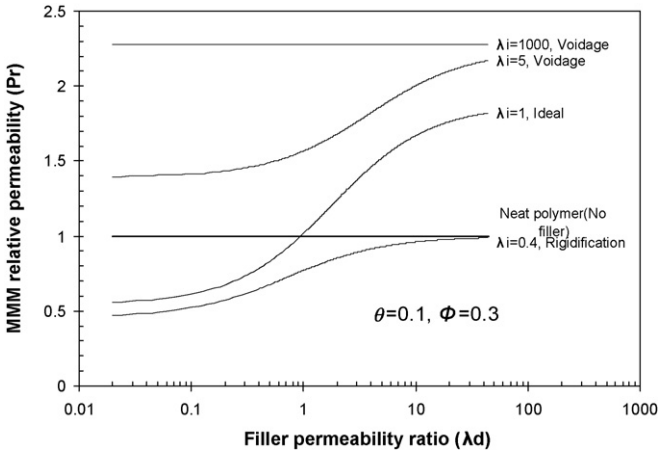

Fig. 11. Effect of dispersed filler permeability ratio and interphase permeability ratio on MMM relative permeability.

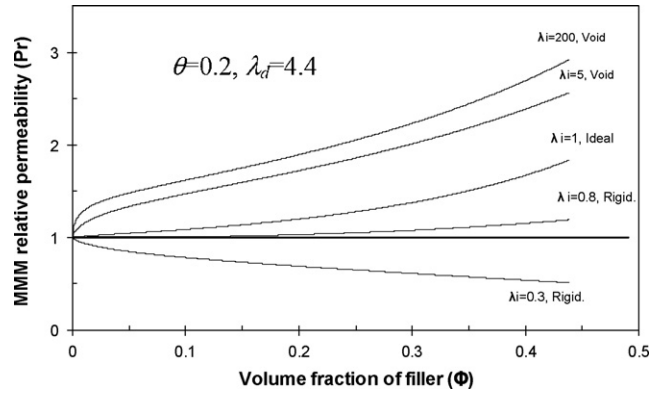

Fig. 12. Effect of filler loading and interphase permeability ratio on MMM relative permeability.

Table 1
Specification of Cases 1–7.

Case no.	Number of data points	P_d (fast gas)	α_d	Filler loading (ϕ)	Filler type	Polymer matrix	Gases	Ref.
1	2	0.77	37	0.20	Zeolite NaA	Matrimid 5218	O_2/N_2	[13]
2	2	0.77	37	0.20	Zeolite NaA	Matrimid 5218	O_2/N_2	[13]
3	6	0.77	37	0.20,0.30,0.40	Zeolite NaA	BAPB–BPADA	O_2/N_2	[14]
4	4	0.77	37	0.15,0.35	Zeolite NaA	Ultem 1000	O_2/N_2	[14]
5	8	44	200	0.17,0.19,0.33,0.36	Carbon molecular sieve	Matrimid 5218	CO_2/CH_4	[41]
6	6	22	13.3	0.17,0.19,0.33,0.36	Carbon molecular sieve	Matrimid 5218	O_2/N_2	[41]
7	8	0.77	37	0.18,0.28,0.38,0.48	Zeolite NaA	Polyethersulfone	O_2/N_2	[42]

(f) Fig. 12 also compares rigidified, ideal, leaky and void in MMM. θ and λ_d are set equal to 0.2 and 4.4, respectively. λ_i is changed progressively from 0.3 (rigidified MMM), 0.8 (rigidified MMM), 1.0 (ideal MMM), 5.0 (leaky MMM) and to 200 (Void in MMM). P_r is shown as a function of ϕ in Fig. 12. From Fig. 12, P_r decreases with an increase in ϕ when λ_i is as low as 0.3. P_r increases with an increase in ϕ when λ_i is either 1.0 (ideal MMM) or 5.0 (leaky MMM) or 200 (Void in MMM). Interestingly, P_r also increases with an increase in ϕ when λ_i equal to 0.8. This is because the high λ_d value (4.4) compensates the low λ_i value.

4.2. Comparison between the proposed model and experimental data

The model was tested by fitting seven sets, called hereafter cases, of experimental data on MMM permeabilities and selectivities that are reported in the literature. Table 1 gives a summary of the cases. As the experimental data the following quantities are considered:

$$\text{Relative permeability of the fast gas} = (P_r)_1 \tag{34}$$

Where the subscript 1 means the fast gas:

$$\text{Relative selectivity} = (\alpha_r)_{1/2} = \frac{(\alpha)_{1/2}}{(\alpha_m)_{1/2}} = \frac{(P)_1/(P)_2}{(P_m)_1/(P_m)_2} = \frac{(P_r)_1}{(P_r)_2} \tag{35}$$

From Eqs. (34) and (35), it is clear that P_r is necessary to be know for both gases 1 and 2. Considering Eq. (33) which was given to a single gas, total 8 parameters are seem to be given before the model is applied. However, two of them, ϕ and θ are common for both gases. Among 6 parameters that are left; i.e. ϕ, $(\lambda_d)_1$, $(\lambda_d)_2$, $(\lambda_i)_1$, $(\lambda_i)_2$ and θ. ϕ, the dispersed filler loading is reported in the literature and listed in Table 1 for each case. λ_d for gas 1 and $(\alpha_d)_{1/2}$ are reported in Table 1. λ_i (P_i) values for gas 1 and 2 are considered here as the fitting parameters in nonlinear regression. θ, which represents the thickness of the interphase, is fixed to 0.1, based on Vu et al.'s work [11] for rigidified MMM, while the value of θ for void in MMM is roughly estimated from FESEM analysis illustrated in the relevant reference (Case 1: $t \approx 03.33 \times 10^{-7}$ m and $d_p = 3.5 \times 10^{-6}$ m from Ref. [14] yields: $\theta \approx 0.10$). For leaky MMM (Case 2), the calculated P_i's are based on $\theta \approx 0.0003$. As it is known, the exact value of interphase thickness hence, θ cannot be detected easily even from FESEM analysis. Therefore we assumed $t = 10$ Å (and $d_p = 3.5 \times 10^{-6}$ m from Ref. [13]), that yields $\theta \approx 0.0003$. It is clear that the calculated P_i's will be different where θ have the other values.

The fitting parameters are tuned by minimizing percentage of average absolute relative error (*%AARE*) as the objective function that is shown by Eq. (36):

$$\%AARE = \frac{100}{NDP}\sum_{j=1}^{NDP}\left|\frac{P_j^{calc} - P_j^{\exp}}{P_j^{\exp}}\right| \tag{36}$$

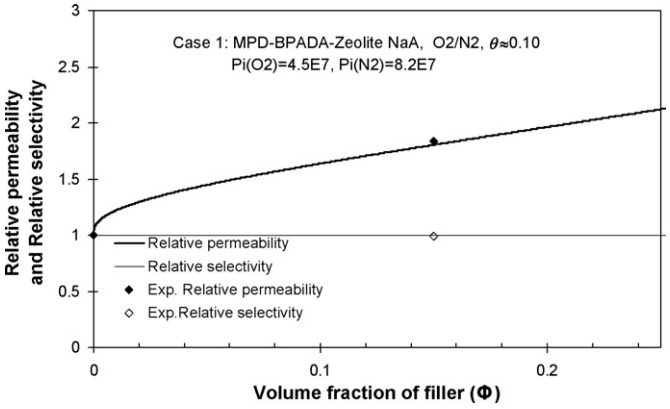

Fig. 13. Model prediction of relative permeability and selectivity versus experimental data for MPD-BPADA–zeolite NaA MMM for O_2/N_2 gas separation.

where $P_j^{\exp}$ is the jth experimental value, and P_j^{calc} is the corresponding calculated value. *NDP* is the number of the data points.

Once optimum values are chosen for λ_is model calculation was done for different ϕ values and the results are presented in Figs. 13–19.

Case 1: The MMM consists of zeolite NaA as the dispersed phase and Matrimid 5218 as the continuous phase. The experimental data were obtained by Mahajan and Koros [14] for O_2/N_2 separation. In the fitting procedure θ was fixed a priori to 0.10. The experimental points are exactly on the calculated lines, see Fig. 13. This is natural since there are two experimental values for two unknown parameters (two λ_is). Hence this is not regression analysis but simultaneous solution of two equations. The very large λ_i values indicate that this case corresponds to void in MMM. Relative selectivity remains unity but relative permeability increases with an increase in ϕ.

Case 2: Mahajan and Koros [13] carried out experiments, using silane agent (aminopropyltriethoxysilane (APTES)) to improve the

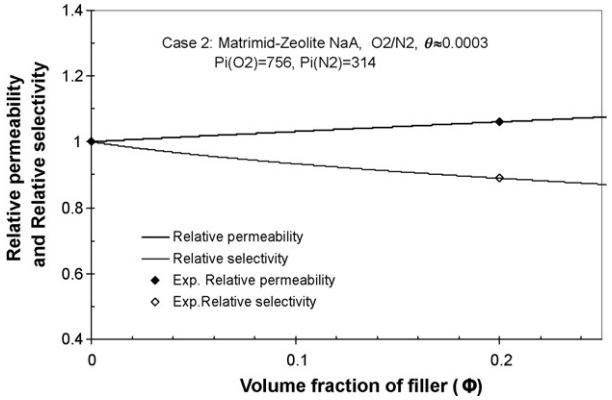

Fig. 14. Model prediction of relative permeability and selectivity versus experimental data for Matrimid–zeolite NaA MMM for O_2/N_2 gas separation.

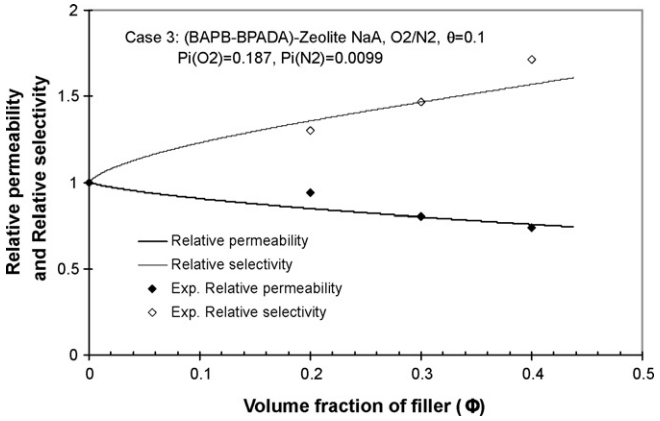

Fig. 15. Model prediction of relative permeability and selectivity versus experimental data for (BAPB–BPADA)–zeolite NaA MMM for O_2/N_2 gas separation.

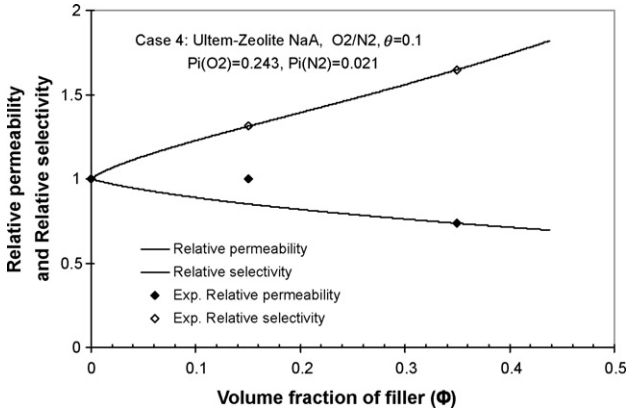

Fig. 16. Model prediction of relative permeability and selectivity versus experimental data for ultem–zeolite NaA MMM for O_2/N_2 gas separation.

zeolite–polymer adhesion. They could decrease the interphase thickness to the order of gas molecular size. Hence, as mentioned above, a very small θ was used in optimization. Since $\theta > 0.0$ and relative selectivity is less than 1 this case corresponds to a leaky MMM. Again, the experimental data are exactly on the calculated line, because the number of the experimental data is two, see Fig. 14.

Case 3: For O_2/N_2 separation Mahajan and Koros [14] proposed a MMM to achieve high selectivity by mixing BAPB–BPADA as polymer matrix and zeolite NaA as filler successfully. Fig. 15 shows good agreement between the proposed model and the experimental data. Since both λ_is are much smaller than unity, Case 3 exhibits

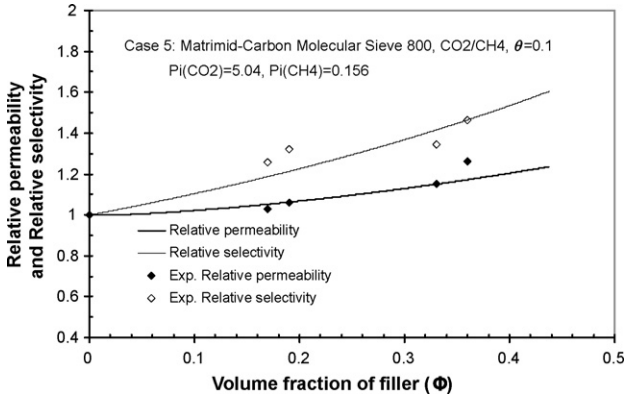

Fig. 17. Model prediction of relative permeability and selectivity versus experimental data for Matrimid-CMS MMM for CO_2/CH_4 gas separation.

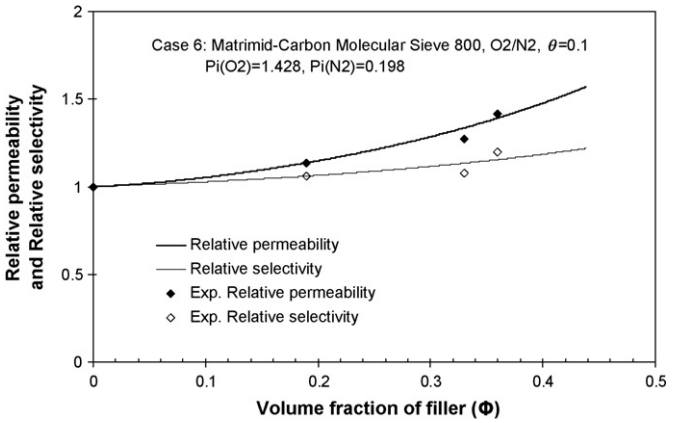

Fig. 18. Model prediction of relative permeability and selectivity versus experimental data for Matrimid-CMS MMM for O_2/N_2 gas separation.

a rigidified MMM.

Case 4: Mahajan and Koros [14] in the next work investigated a MMM of ultem/zeolite NaA for O_2/N_2 separation. Fig. 16 shows good agreement between the model calculation and the experimental data. Since both λ_i values are less than 1.0, Case 4 is rigidified MMM.

Case 5: Vu et al. [41] investigated MMM of Matrimid/carbon molecular sieve (CMS) system for CO_2/CH_4 separation. As can be seen from Table 1, CMS has prominent properties for CO_2/CH_4 separation. Fig. 17 compares the model predictions with the experimental data. The model describes the experimental data reasonably well. Since λ_is are less than unity Case 5 is a rigidified MMM. Interestingly, unlike Cases 3 and 4, relative permeability, together with relative selectivity, increases with an increase in ϕ. This is because of very high λ_d values. As well, λ_i values are not much smaller than unity. Hence this case is close to ideal MMM.

Case 6: For the same Matrimid/CMS system for O_2/N_2 separation [41], Fig. 18 shows reasonable agreement between the model predictions and the experimental data. Case 6 is similar to Case 5 in its behavior. Hence this case is rigidified MMM but close to ideal MMM.

Case 7: For O_2/N_2 separation by polyethersulfone/zeolite NaA MMM [42], Fig. 19 shows excellent agreement between the proposed model and the experimental data. Similar to Cases 3 and 4, Case 7 has typical characteristics of a rigidified MMM. Most interestingly, the highest value of ϕ involved in this case is 0.48, which is higher than the theoretical closest packing of 0.394, which proves

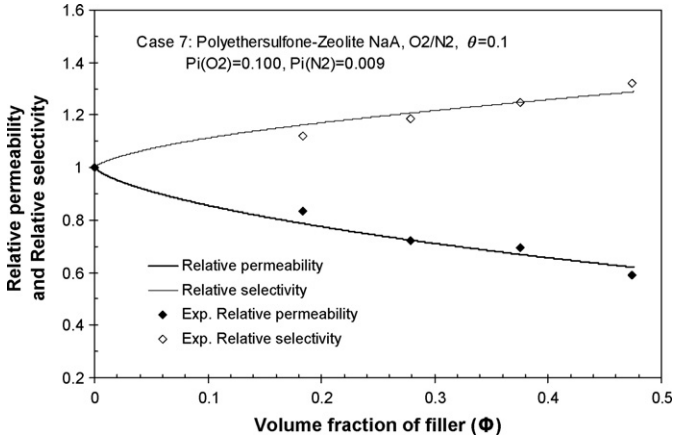

Fig. 19. Model prediction of relative permeability and selectivity versus experimental data for polyethersulfone–zeolite NaA MMM for O_2/N_2 gas separation.

strong prediction capacity of this model. It should be noted however that, for practical applications, MMMs with filler loadings higher than 0.4 are rarely successful due to their high brittleness [14].

5. Conclusions

A new theoretical model based on resistance modeling approach was developed to describe the permeability and selectivity of MMM systems. The proposed model predicted MMM permeability directly, by taking into consideration the presence of interphase thickness around the filler particle. The new model was able to give the true trend of MMM permeability relative to change in the main parameters. Moreover, the proposed model was capable to predict permeability and selectivity of MMM systems, not only at low filler loading values but also at higher values of filler loading. Generally, the model had the ability to cover all the MMM morphologies and there was a high degree of agreement between model predictions and published experimental data. The proposed model is capable to give a useful tool to enhance our knowledge related to the gas flow behavior and hence distinguishing the differences between the morphologies and their influences on gas permeabilities in MMM.

Nomenclature

a, b, c	MMM element dimensions
A	membrane area
AARE	average absolute relative error
d	particle diameter or height
l	membrane thickness
NDP	number of data points
P	permeability
p	gas pressure
Q	gas volumetric flow rate
R	permeance resistance
t	interphase thickness
u	parameter in the developed model

Greek letters

α	permselectivity
β	ratio of the interphase permeability to the polymer permeability
δ	ratio of the interphase radius to the particle radius, particle size
Δ	difference in pressure
ϕ	filler loading
ϕ'	dimension parameters in developed model
γ	ratio of the interphase thickness to the particle radius
λ	permeability ratio

Superscripts

calc	calculated
exp	experimental
i	interphase

Subscripts

d	dispersed phase
i	interphase
j	counter
m	polymer matrix
r	relative
S	inorganic phase in the combined inorganic and interphase phase
I, II, III	element different regions
1,2	penetrant gas through membrane

References

[1] P. Pandey, R.S. Chauhan, Membranes for gas separation, Prog. Polym. Sci. 26 (2001) 853–893.
[2] H. Lin, B.D. Freeman, Materials selection guidelines for membranes that remove CO_2 from gas mixtures, J. Mol. Struct. 739 (2005) 57–74.
[3] E.F. McLeary, J.C. Jansen, F. Kapteijn, Zeolite based films, membranes and membrane reactors: progress and prospects, Micropor. Mesopor. Mater. 90 (2006) 198–220.
[4] T.S. Chung, L.Y. Jiang, S. Kulprathipanja, Mixed matrix membranes (MMMs) comprising organic polymers with dispersed inorganic fillers for gas separation, Prog. Polym. Sci. 32 (2007) 483–507.
[5] R. Mahajan, W.J. Koros, M. Thundyil, Mixed matrix membranes: important and challenging!, Membr. Technol. 105 (1999) 6–8.
[6] T.T. Moore, R. Mahajan, D.Q. Vu, W.J. Koros, Hybrid membrane materials comprising organic polymers with rigid dispersed phases, AIChE J. 50 (2004) 311–321.
[7] R.H.B. Bouma, A. Checchetti, G. Chidichimo, E. Drioli, Permeation through a heterogeneous membrane: the effect of the dispersed phase, J. Membr. Sci. 128 (1997) 141–149.
[8] C.M. Zimmerman, A. Singh, W.J. Koros, Tailoring mixed matrix composite membranes for gas separations, J. Membr. Sci. 137 (1997) 145–154.
[9] E.E. Gonzo, M.L. Parentis, J.C. Gottifredi, Estimating models for predicting effective permeability of mixed matrix membranes, J. Membr. Sci. 277 (2006) 46–54.
[10] T.W. Pechar, M. Tsapatsis, E. Marand, R. Davis, Preparation and characterization of a glassy fluorinated polyimide zeolite-mixed matrix membrane, Desalination 146 (2002) 3–9.
[11] D.Q. Vu, W.J. Koros, S.J. Miller, Mixed matrix membranes using carbon molecular sieves. II. Modeling permeation behaviour, J. Membr. Sci. 211 (2003) 335–348.
[12] R. Mahajan, W.J. Koros, Factors controlling successful formation of mixed-matrix gas separation materials, Ind. Eng. Chem. Res. 39 (2000) 2692–2696.
[13] R. Mahajan, W.J. Koros, Mixed matrix membrane materials with glassy polymers. Part I, Polym. Eng. Sci. 42 (2002) 1420–1431.
[14] R. Mahajan, W.J. Koros, Mixed matrix membrane materials with glassy polymers. Part II, Polym. Eng. Sci. 42 (2002) 1432–1441.
[15] Y. Li, B. Krantz, T.S. Chung, A novel primer to prevent nanoparticle agglomeration in mixed matrix membranes, AIChE J. 53 (2007) 2470–2475.
[16] L.Y. Jiang, T.S. Chung, R. Rajagopalan, Matrimid®/MgO mixed matrix membranes for pervaporation, AIChE J. 53 (2007) 1745–1757.
[17] Y. Li, T.S. Chung, S. Kulprathipanja, Novel Ag^+–zeolite/polymer mixed matrix membranes with a high CO_2/CH_4 selectivity, AIChE J. 53 (2007) 610–616.
[18] S. Sridhar, B. Smitha, T.M. Aminabhavi, Separation of carbon dioxide from natural gas mixtures through polymeric membranes—a review, Sep. Purif. Rev. 36 (2007) 113–174.
[19] S.B. Teli, G.S. Gokavi, M. Sairam, T.M. Aminabhavi, Mixed matrix membranes of poly(vinyl alcohol) loaded with phosphomolybdic heteropolyacid for the pervaporation separation of water–isopropanol mixtures, Colloids Surf. A 301 (2007) 55–62.
[20] J.A. Sheffel, M. Tsapatsis, A model for the performance of microporous mixed matrix membranes with oriented selective flakes, J. Membr. Sci. 295 (2007) 50–70.
[21] R.B. Qi, Y.J. Wang, J. Chen, J.D. Li, S.L. Zhu, Removing thiophenes from n-octane using PDMS–AgY zeolite mixed matrix membranes, J. Membr. Sci. 295 (2007) 114–120.
[22] T.T. Moore, W.J. Koros, Gas sorption in polymers, molecular sieves, and mixed matrix membranes, J. Appl. Polym. Sci. 104 (2007) 4053–4059.
[23] A.F. Ismail, R.A. Rahim, W.A.W.A. Rahman, Characterization of polyethersulfone/Matrimid® 5218 miscible blend mixed matrix membranes for O_2/N_2 gas separation, Sep. Purif. Technol. 63 (2008) 200–206.
[24] A.F. Ismail, T.D. Kusworo, A. Mustafa, Enhanced gas permeation performance of polyethersulfone mixed matrix hollow fiber membranes using novel Dynasylan Ameo silane agent, J. Membr. Sci. 319 (2008) 306–312.
[25] W.A.W. Rafizah, A.F. Ismail, Effect of carbon molecular sieve sizing with poly(vinyl pyrrolidone) K-15 on carbon molecular sieve–polysulfone mixed matrix membrane, J. Membr. Sci. 307 (2008) 53–61.
[26] J.D. Felske, Effective thermal conductivity of composite spheres in a continuous medium with contact resistance, Int. Heat Mass Transfer 47 (2004) 3453–3461.
[27] R. Pal, Permeation models for mixed matrix membranes, J. Colloid Interface Sci. 317 (2008) 191–198.
[28] J.M.S. Henis, M.K. Tripodi, Composite hollow fiber membranes for gas permeation: the resistance model approach, J. Membrane Sci. 8 (1981) 233–246.

[29] A. Fouda, Y. Chen, J. Bai, T. Matsuura, Wheatstone bridge model for the laminated polydimethylsiloxane/polyethersulfone membrane for gas separation, J. Membr. Sci. 64 (1991) 263–271.
[30] S.K. Karode, V.S. Patwardhan, S.S. Kulkarni, An improved model incorporating constriction resistance in transport through thin film composite membranes, J. Membr. Sci. 114 (1996) 157–170.
[31] C.V. Funk, D.R. Lloyd, Zeolite-filled microporous mixed matrix (ZeoTIPS) membranes: prediction of gas separation performance, J. Membr. Sci. 313 (2008) 224–231.
[32] J.C. Maxwell, A Treatise on Electricity and Magnetism, Dover Publications, New York, 1954.
[33] D.A.G. Bruggeman, Berechnung Verschiedener Physikalischer Konstanten Von Heterogenen Substanzen. I. Dielektrizitatskonstanten Und Leitfahigkeiten Der Mischkorper Aus Isotropen Substanzen, Ann. Phys. 24 (1935) 636–679.
[34] T.B. Lewis, L.E. Nielsen, Dynamic mechanical properties of particulate-filled composites, J. Appl. Polym. Sci. 14 (1970) 1449–1471.
[35] R. Pal, New models for thermal conductivity of particulate composites, J. Reinf. Plast. Compos. 26 (2007) 643–651.
[36] C.J.F. Bottcher, The dielectric constant of crystalline powders, Recueil des Travaux Chimiques des Pays-Bas 64 (1945) 47–51.
[37] W.I. Higuchi, T. Higuchi, Theoretical analysis of diffusional movement through heterogeneous barriers, J. Am. Pharm. Assoc. Sci. Ed. 49 (1960) 598.
[38] S.A. Hashemifard, A.F. Ismail, T. Matsuura, Prediction of gas permeability in mixed matrix membranes using theoretical models, J. Membr. Sci. (2008), doi:10.1016/j.memsci.2009.10.005.
[39] J.H. Petropoulos, A comparative study of approaches applied to the permeability of binary composite polymeric materials, J. Polym. Sci. Polym. Phys. Ed. 23 (1985) 1309–1324.
[40] T.T. Moore, W.J. Koros, Non-ideal effects in organic–inorganic materials for gas separation membranes, J. Mol. Struct. 739 (2005) 87–98.
[41] D.Q. Vu, W.J. Koros, S.J. Miller, Mixed matrix membranes using carbon molecular sieves I. Preparation and experimental results, J. Membr. Sci. 211 (2003) 311–334.
[42] Y. Li, T.S. Chunga, C. Caoa, S. Kulprathipanj, The effects of polymer chain rigidification, zeolite pore size and pore blockage on polyethersulfone (PES)–zeolite A mixed matrix membranes, J. Membr. Sci. 260 (2005) 45–55.